American Mineralogist, Volume 81, pages 158–168, 1996

Morphology and maturation of melt inclusions in quartz phenocrysts from the Badlands rhyolite lava flow, southwestern Idaho

CURTIS R. MANLEY

Department of Geology, Box 871404, Arizona State University, Tempe, Arizona 85287-1404, U.S.A.

ABSTRACT

Morphologies of primary rhyolitic melt inclusions in three successive populations of quartz phenocrysts in a single volcanic unit illustrate the change of inclusion shape after trapping. The 14 Ma Badlands lava flow on the Owyhee Plateau of southwestern Idaho contains two magmas with three distinct quartz populations differing in size and morphology. In tiny quartz crystals that nucleated shortly before the eruption, large melt inclusions retain their initial, irregular shapes, whereas the smallest inclusions show mature negative crystal shapes. Inclusions in a population of larger quartz crystals that nucleated earlier all show either negative crystal shapes or faceted shapes transitional to negative crystals. All inclusions in a third population of large corroded quartz crystals have mature negative crystal shapes regardless of inclusion size. In silicic magmatic systems, irregularly shaped inclusions in quartz may imply trapping just before eruption; analyses of such inclusions should have the greatest likelihood of revealing the magmatic volatile conditions driving the eruption.

Electron microprobe analyses show that maturation had no effect on the composition of the trapped melt. After eruption, however, slow cooling led to coarse crystallization and loss of silica from the melt; when these inclusions were revitrified in the laboratory, they did not regain all lost silica and did not become completely homogeneous. Revitrification of inclusions that cooled more quickly showed no such loss of silica to the host. Thus, given appropriate cooling conditions, even very old (Precambrian?) silicic melt inclusions may be suitable for microbeam analysis after any necessary revitrification in the laboratory.

INTRODUCTION

Microbeam analytical techniques have dramatically increased the usefulness of igneous silicate melt inclusions for determining the original volatile contents, compositions, and temperatures of erupted magmas. To exploit fully the information recorded in melt inclusions, we need to understand the inclusions' probable morphology and composition at the time of their trapping and how these may have changed after entrapment. Such information has the potential to provide better constraints on magmatic evolution and crystallization processes, triggering of eruptions, and eruption dynamics.

Most of what we know about the processes of trapping of fluid and melt inclusions has been gained from microscopic study of natural inclusions and more directly by laboratory observations of crystal growth and fluid-inclusion formation in relatively low-temperature aqueous systems. Primary inclusions, which are trapped during growth of the surrounding host crystal (see discussion in Roedder 1984), form because of a variety of conditions, including defects in crystal growth, such as kinking of a new growth layer over a planar crystal face (Sisson et al. 1993), and localized temporary stagnation of growth causing depressions or hollows that are covered by subsequent growth (Wilkins 1979). This is in contrast to secondary inclusions, which are trapped, in either fractures (see Roedder 1984) or dissolved reentrants (Donaldson and Henderson 1988), after the crystal has formed.

Primary fluid and melt inclusions are thought to be trapped only very rarely with negative crystal shapes (Roedder 1984). Sisson et al. (1993) observed irregular primary fluid inclusions forming in laboratory experiments, but the temperatures and conditions involved in trapping of primary melt inclusions have so far precluded direct observation of their formation. In the laboratory, synthetic, secondary inclusions of aqueous fluid, formed along fractures in quartz, are commonly observed to neck down into many smaller, isolated inclusions with more regular shapes by local dissolution and reprecipitation of quartz (Shelton and Orville 1980; Roedder 1984). Likewise, the regular shapes of most primary melt inclusions are thought to result from posttrapping evolution or maturation of their morphology to minimize surface energy (Chaigneau et al. 1980; Beddoe-Stephens et al. 1983; Roedder 1984). This maturation often yields inclusions with the spherical (lowest surface area per volume) or negative crystal shapes (lowest surface energy) most often

0003–004X/96/0102–0158$05.00

seen in igneous phenocrysts (Roedder 1984). Maturation occurs only if temperature conditions remain suitable; for example, Clocchiatti (1975) reported that a rounded melt inclusion in quartz developed a negative crystal shape after it was held at 700–800 °C for six weeks. Experimental studies at 900 °C and 1 GPa (Laporte and Provost 1994) indicate that the equilibrium shape (no net growth, no net dissolution; see Wortis 1988) of a quartz crystal in a silicate liquid is a bipyramid with pristine, flat faces but with smooth apices and interfacial edges. This is also the morphology of most melt inclusions with negative crystal shapes in igneous quartz phenocrysts, i.e., smooth, lacking sharp angles and terminations.

It is generally assumed that maturation involves only the redistribution of material of the host crystal, with no net loss or gain of chemical components from the inclusion fluid as the shape of the inclusion changes. This is most easily shown for synthetic, secondary inclusions of aqueous fluid, where the composition of the fluid is very different from that of the host quartz. In contrast, rhyolitic melt inclusions have high SiO_2 contents in common with their quartz and feldspar hosts, and more mafic melts share more elements with their pyroxene and olivine hosts.

The initial shapes of igneous melt inclusions, and how these then change with maturation, are nicely illustrated by rhyolitic melt inclusions in successively nucleated populations of quartz phenocrysts in the Badlands lava flow of southwestern Idaho.

Geological context of samples

The Badlands lava flow is a rhyolitic unit with a total known volume of about 15 km³ (Manley 1994, 1995). It is associated with other large-volume rhyolite lavas and ignimbrites erupted between 14 and 9 Ma (Bonnichsen 1982a, 1982b; Ekren et al. 1984; Bonnichsen and Kauffman 1987) when the Yellowstone hotspot was located beneath what is now the southwestern corner of Idaho, also known as the Owyhee Plateau.

The main events during the Badlands eruption, which tapped two distinct types of magma, can be determined from field relations in the unit's well-exposed vent area (Fig. 1; Manley 1994, 1995). A dike at least 5–10 km long (in plan view) propagated to the surface, and the first surficial activity involved minor extrusion of aphyric lava at the dike termination and sub-Plinian explosive eruptions from the main eruptive fissures, which built up ~50 m thick ridges of nonwelded tephra representing mixed aphyric and phenocryst-rich magma. The narrow dike termination probably quickly became inactive because of rapid cooling (e.g., Delaney and Pollard 1981). When explosive activity ceased, lava effusion began. Near the dike termination, aphyric and phenocryst-rich magmas mingled during ascent and emplacement; the majority of the multilobed 15 km³ Badlands lava is composed of the phenocryst-rich material.

The predominant Badlands magma, a phenocryst-rich (30 vol%) rhyolite (~75 wt% SiO_2, Table 1), had an anhydrous mineral assemblage of quartz + sanidine + plagioclase + augite + orthopyroxene + magnetite + ilmenite. The matrix melt was a silica-rich rhyolite (sample 89–153-ts, Table 1). Compositions of coexisting feldspar and pyroxene phenocrysts (Fuhrman and Lindsley 1988; Andersen et al. 1993) indicate a probable eruption temperature of about 830 ± 30 °C (Manley 1994).

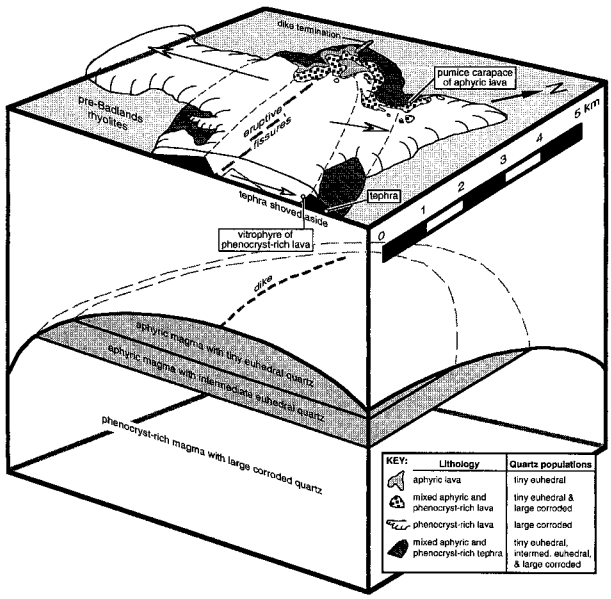

Figure 1. Perspective drawing of the exposed vent area of the Badlands lava flow, showing distribution of the aphyric and phenocryst-rich lithologies. Effusive aphyric lava is primarily found in the narrow dike termination and the portion of the flow front closest to it. Cross-sectional views of the wedge-shaped tephra deposits are shown in black. The northeastern tephra deposit was shoved aside by the weight of the spreading lava flow. Lines from boxes show locations of samples from which quartz phenocrysts were separated for this study. Also shown is the inferred preeruption geometry of layering in the Badlands magma chamber, based on field and petrologic relations in the tephra deposits and lava flow. Two layers of aphyric magma overlie the main volume of phenocryst-rich magma. Eruptive tapping presumably occurred through dikes that propagated upward from the top of the chamber ("footprint" of dike is shown on roof of chamber; dike omitted for clarity).

The nearly aphyric magma was a crystal-poor (<0.5 vol%), silica-rich rhyolite (~77 wt% SiO_2, Table 1) with a mineral assemblage of small euhedral crystals of quartz + sanidine + plagioclase + biotite + hornblende + magnetite + ilmenite (Manley 1994). Compositions of the coexisting iron titanium oxide phenocrysts (see Andersen et al. 1993) indicate a probable eruption temperature of about 820 ± 30 °C (Manley 1994); compositions of coexisting feldspar phenocrysts do not converge to a meaningful temperature using the approach of Fuhrman and Lindsley (1988).

The initial explosive phase of the eruption preferentially tapped the aphyric magma, but phenocrysts of all magma types are represented in individual beds of the tephra. Although the later effusive phase was dominated

TABLE 1. Compositions of bulk lava and matrix glass samples

	Bulk samples		Matrix glasses	
Sample	Phenocryst-rich 90-177R	Aphyric 90-188	Phenocryst-rich 89-153-ts	Aphyric 90-188-G1
Material	Vitrophyre	Obsidian	Matrix glass	Obsidian
Analysis			17	27
SiO_2	75.1	76.7	76.5	76.4
TiO_2	0.313	0.116	0.14	0.08
Al_2O_3	12.7	12.3	12.2	12.3
Fe_2O_3*	1.95	1.11	1.60	1.23
MnO	0.031	0.023	0.05	<0.05
MgO	0.12	0.00	0.03	<0.01
CaO	1.03	0.62	0.51	0.55
Na_2O	2.90	3.59	3.29	3.71
K_2O	5.79	5.31	5.25	5.26
P_2O_5	0.048	0.011	0.03	<0.03
Cl	n.a.	0.08	0.08	0.07
F	n.a.	0.14	0.32	0.39
Total	99.03	99.59	98.38	100.65
H_2O	n.a.	n.a.	1.91**	0.10†

Note: Analyses recalculated to 100% anhydrous; totals are those before normalization. H_2O analyses by secondary ion mass spectrometry (ion microprobe; see Hervig et al. 1989); all other oxides by wavelength-dispersive X-ray fluorescence spectroscopy (bulk samples) or electron microprobe (matrix glasses). All data in weight percent; n.a. = not analyzed.

* Total Fe as Fe_2O_3.

** This is secondary water of meteoric origin in the hydrated (perlitic) glass.

† This is juvenile water of magmatic origin in the pristine glass (obsidian).

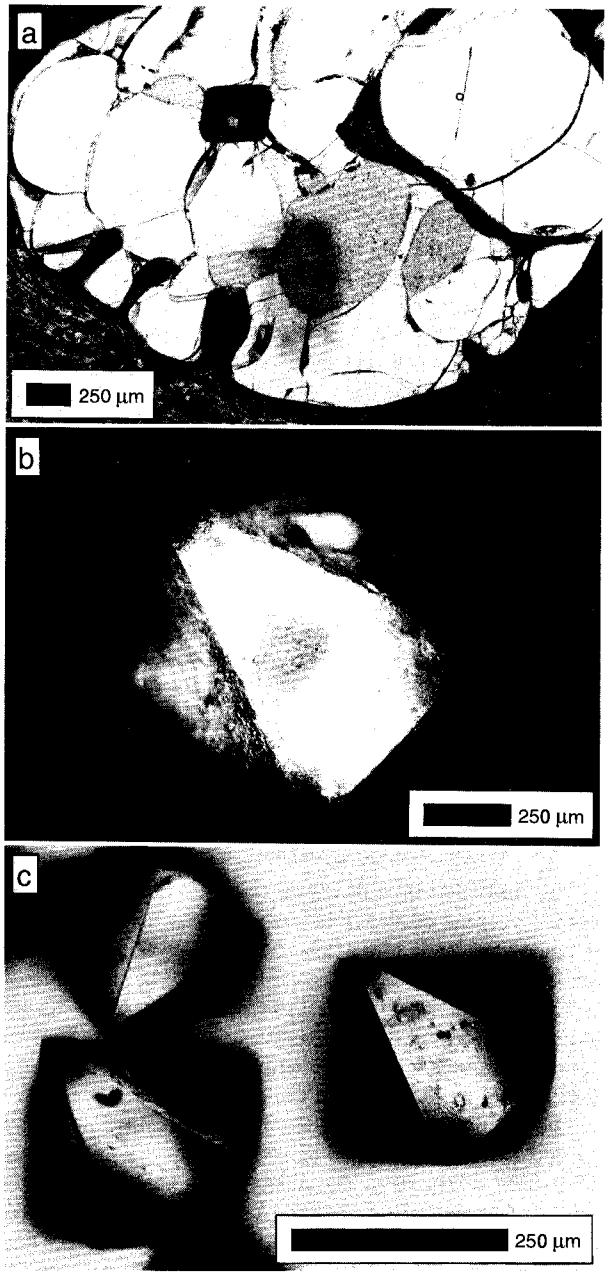

→

FIGURE 2. Transmitted-light photomicrographs of representative grains from the three populations of quartz phenocrysts shown in the histogram in Figure 3. Note different scales. (**a**) Thin-section view of a large corroded quartz phenocryst in the Badlands lava-flow vitrophyre. The crystal shows curved fractures and embayments (lower left) filled with matrix glass. In upper left is a large crystallized (black) melt inclusion with negative crystal shape. Areas of speckled gray within the phenocryst were plucked during thin-section preparation. Field of view is 3.25 mm. (**b**) Bipyramidal intermediate euhedral quartz crystal, lying on its side. Note smooth apex, rough appearance of faces, and slight reentrant (out of focus) on face at top. Crystal was not acid cleaned. Field of view is 1.625 mm. (**c**) Three bipyramidal, tiny euhedral quartz crystals. Note sharp interfacial edges and apices, and pristine faces; material on faces is adhering glassy matrix (crystals were not acid cleaned). Field of view is 0.65 mm.

by the phenocryst-rich magma, it began with effusion of a small volume of the aphyric magma near the termination of the dike. The field and petrographic relations indicate that a small body (a layer or a cupola) of the aphyric magma must have overlain the phenocryst-rich magma in the chamber at the beginning of the eruption (Manley 1994, 1995). With the assumption that the chamber was tapped near its apex, mixing of the magma types during the initial explosive phase likely involved draw-up of the underlying magma layers (i.e., Blake and Ivey 1986). The apparent stratified chamber geometry and the aphyric magma's low crystal content and major and trace element compositional similarity to the matrix liquid of the phenocryst-rich magma (Manley 1994) imply that the aphyric magma evolved from the phenocryst-rich magma; the small euhedral phenocrysts in the aphyric magma nucleated and grew there; they were not inherited from the phenocryst-rich magma. The rise of an evolved, less-dense, H_2O-rich melt along the magma-chamber wall (McBirney 1980; Turner and Gufstafson 1981), accumulating at the chamber top, is consistent with the field and petrologic constraints.

METHODS

Sample preparation

All quartz phenocrysts were collected from the Badlands rhyolite unit; they were separated from hydrated

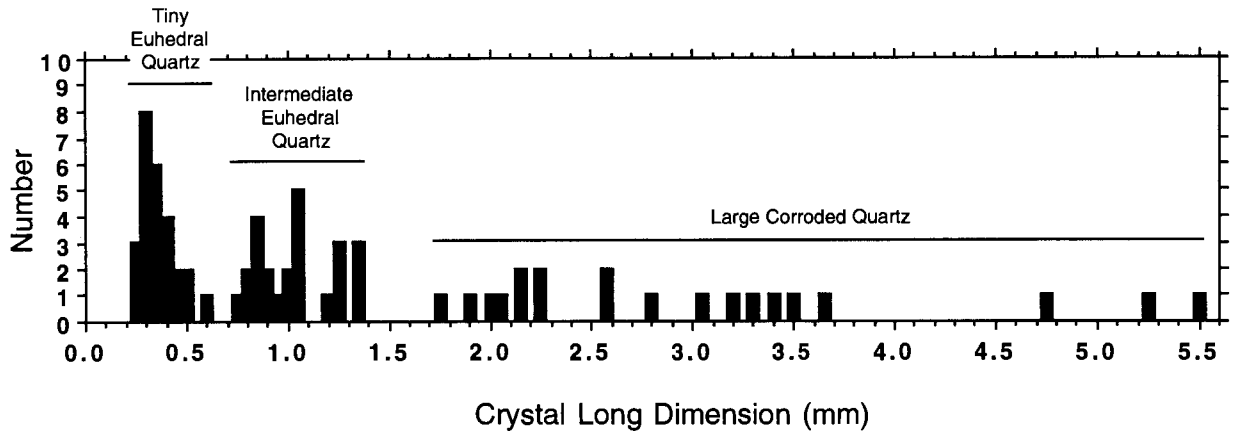

FIGURE 3. Histogram showing the sizes of quartz phenocrysts separated from various samples of the Badlands rhyolite unit. The crystals fall into three discrete, nonoverlapping populations: tiny euhedral bipyramidal quartz (250–580 μm in length; $n = 26$ crystals), intermediate euhedral bipyramidal quartz (750–1375 μm; $n = 24$), and large corroded quartz (1750–5500 μm; $n = 20$ nonfragmented crystals). The similar sizes and morphologies of the tiny and intermediate euhedral quartz demonstrate that they are closely related.

(perlitic) lava-flow vitrophyre, oxidized lava-flow carapace (surficial) pumice, and zeolitized ashy tephra by gentle crushing, followed by hand-picking. The crystals were cleaned by hand and in an ultrasonic water bath; no acids or solvents were used. Separates of quartz were immersed in mineral oil and inspected for uncracked melt inclusions sufficiently large for microbeam analysis. Crystals with uncracked devitrified melt inclusions were revitrified in the laboratory, generally at atmospheric pressure and ~900 °C; crystals with glassy melt inclusions were not heated. The crystals were then individually mounted in Araldite epoxy disks and polished with emery paper and diamond powder (both with distilled water) to expose the inclusion glass.

Microbeam analyses

For all compositionally analyzed inclusions, ion microprobe analysis was performed only after electron microprobe analysis. The samples were coated with carbon prior to electron microprobe analysis; this coating was then removed by gentle polishing with <2 μm diamond powder and distilled water and replaced with a gold-palladium coating for ion microprobe analysis. The diameter of the primary ion beam was approximately 20 μm during the time of this study; other ion microprobe techniques at Arizona State University are described in Hervig et al. (1989). Electron microprobe analyses were performed with a 15 kV, 10 nA beam with a diameter of 20 μm to minimize loss of Na.

QUARTZ POPULATIONS AND MELT-INCLUSION MORPHOLOGIES

Three distinct populations of quartz phenocrysts (Figs. 2 and 3) were found in the tephras and lavas of the Badlands unit. The phenocryst-rich magma contained large corroded and fractured quartz phenocrysts (up to many millimeters in size), and different portions of the aphyric magma grew two distinct populations of euhedral quartz phenocrysts of different sizes, intermediate (750–1375 μm) and tiny (250–580 μm).

Because all the host crystals are magmatic quartz, and all the trapped liquids are silica-rich rhyolites, chemical and nucleation effects on melt-inclusion morphologies across the three host populations should be minimal. The two populations of euhedral quartz crystallized from essentially the same melt at the same temperature and likely at very similar rates, implying that the melt inclusions in both populations were probably trapped by the same processes and originally had the same morphologies. The growth history of the larger, corroded quartz crystals was probably similar, but there is no way to be certain of this.

Large corroded quartz crystals

The quartz phenocrysts in the phenocryst-rich portion of Badlands lava are spheroids ranging up to at least 5.5 mm in length (Figs. 2a and 3); they are also found in the lithologically mixed tephra vented at the beginning of the eruption. These large quartz phenocrysts have been extensively dissolved, and many show variously sized reentrants or embayments (Donaldson and Henderson 1988) filled with melt (now glass). None of the embayments seem to have been resealed by later growth of the outer crystal surface. These crystals (as well as associated large feldspars, often found in glomerocrysts) are highly fractured, but most fractures annealed or were never throughgoing, as the majority of crystals are intact. Dissolution was enhanced where these fractures intersect the crystal surface, creating troughs that crisscross the surface; many of the reentrants follow these fractures into the crystals. These observations imply that fracturing and dissolution occurred significantly before the eruption and did not result from the energetics of the eruption itself or from decompression (i.e., Nelson and Montana 1992) related to the rise of the magma toward the surface during eruption.

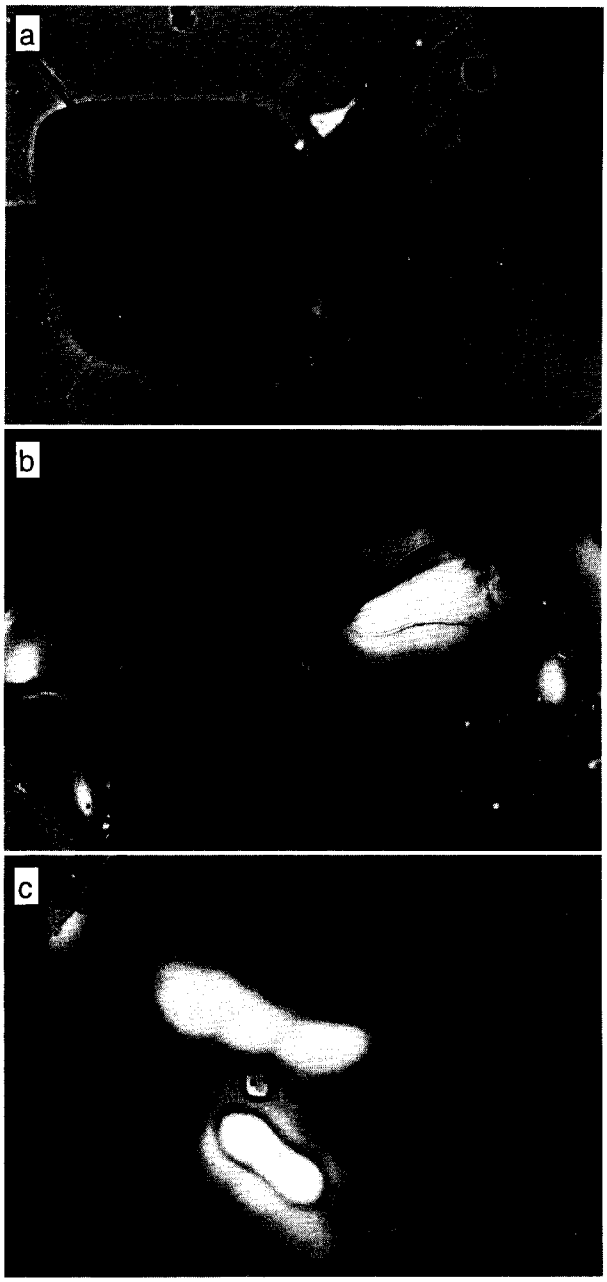

FIGURE 4. Melt inclusions in the intermediate and tiny euhedral quartz crystals. Transmitted-light photomicrographs of inclusions in mounted and polished quartz crystals. All samples were coated with gold-palladium; the bright areas show where this coat was sputtered away by the primary beam of the ion microprobe. Field of view in each figure is 0.325 mm. (**a**) Large melt inclusion of negative crystal shape, exposed at surface of a sample of intermediate euhedral quartz. This inclusion was quenched to glass during the eruption, and thus revitrification was not performed in the laboratory; the glass is brown, and the lighter area within the inclusion is the ion-beam scar through the gold-palladium coating. Smaller, well-faceted inclusions with negative crystal shapes are just below plane of focus in upper right. The fractures were observed forming during sample polishing. Sample 225-Q3. (**b**) Two large irregular melt inclusions exposed at surface of a sample of tiny euhedral quartz. Some slight faceting of the inclusion outline is apparent. The shape of the inclusion that is out of focus in upper left is shown in Figure 5. Formation of the fractures was observed during sample polishing. Opposite crystal faces can be seen in the upper right and the lower left. Melt inclusions were originally finely crystalline and were revitrified at 900 °C at atmospheric pressure. Sample 314-Q2. (c) One large "peanut shell"–shaped irregular melt inclusion is exposed (bright, ion-sputtered area in lower center) at surface of a sample of tiny euhedral quartz (larger bright area is a trail of ion-probe scars on the quartz host). Smaller inclusions with negative crystal shapes can be seen above and to the right of the irregular inclusion. On the right is a partly annealed fracture associated with two ovoid, coarsely crystalline inclusions that did not successfully revitrify (far right, with large vapor bubble; top center, dark, out of focus). Two adjoining crystal faces can be seen on left. Melt inclusion was originally finely crystalline and was revitrified at 900 °C at atmospheric pressure. See drawings in Figure 5. Sample 314-Q4.

←

All melt inclusions in the large corroded quartz phenocrysts have smooth, bipyramidal, negative crystal shapes, which often appear rhombus-shaped or nearly square in plan view under a microscope (see Fig. 4a and photographs in Skirius et al. 1990). The maximum size of these inclusions is 190 × 180 μm. Many of the largest inclusions in these crystals are cut by fractures and have leaked and devitrified as a result.

Intermediate euhedral quartz crystals

A second population of quartz phenocrysts, so far found only in the explosively erupted tephra dominated by the aphyric magma, is of euhedral bipyramidal crystals that were partially dissolved or equilibrated (Fig. 2b); they range from 750 to 1375 μm in length (Fig. 3). Primary crystal-growth faces are apparent on all these crystals, but they have been slightly dissolved and are no longer pristine; apices and interfacial edges have been smoothed by either dissolution (due to changing external conditions) or change in shape of the crystal as it began to minimize its surface energy (Wortis 1988; Laporte and Provost 1994). A few crystals show hollows at the centers of pyramidal faces; though the locations of these features suggest they may have initiated by starvation of the center of the crystal face during growth (Clocchiatti and Basset 1978; Wilkins 1979), they appear to have been deepened and roughened by the dissolution that affected the rest of the crystal's surfaces.

One-half dozen melt inclusions with shapes presumably transitional between irregular and negative crystal shapes (elongate, but with faint facets; Fig. 5) were noted in the intermediate euhedral quartz phenocrysts; these range from 50 × 10 μm to 190 × 80 μm in size (Fig. 6b). All other inclusions, ranging from 190 × 165 μm to 2.5 × 2.5 μm (Fig. 6b), show the same smooth, bipyramidal, negative crystal shapes (Fig. 4a) seen in the large corroded quartz crystals.

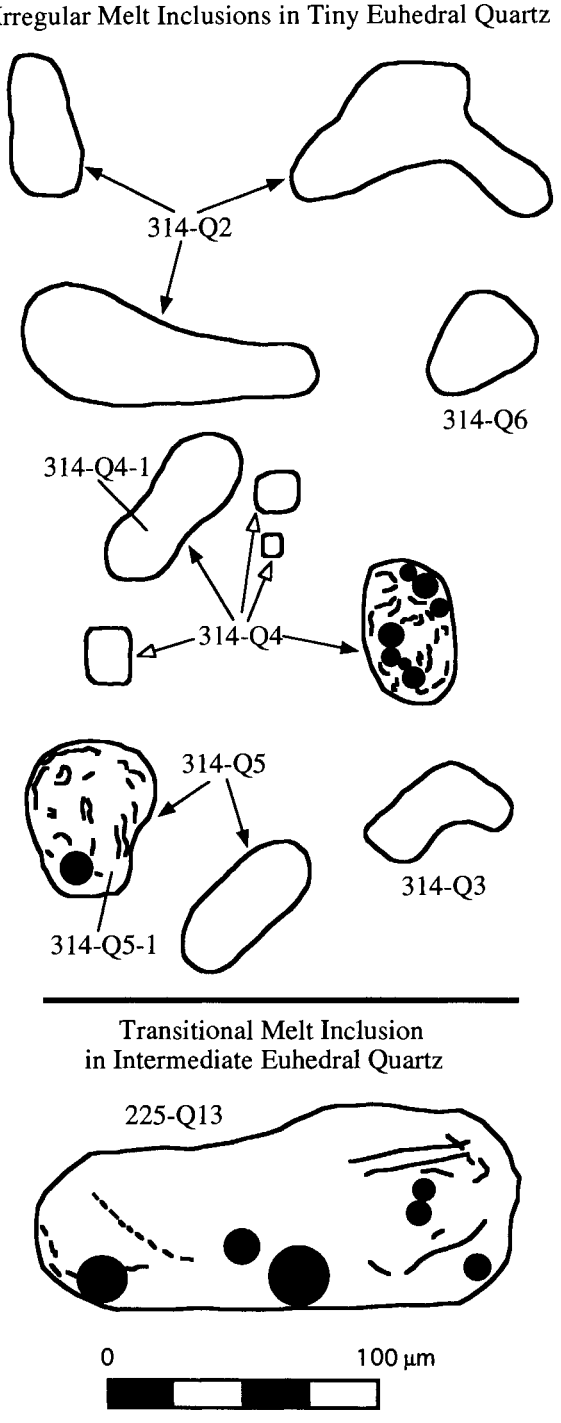

FIGURE 5. Shapes of rhyolitic melt inclusions from the Badlands unit. Line drawings traced from photomicrographs of the plan view (under a microscope) shapes of rhyolitic melt inclusions from two of the Badlands quartz phenocryst populations. Groups of inclusions from a common quartz crystal are indicated by arrows; arrangement of inclusions within a group reflects their relative positions in the crystal. Open arrows indicate inclusions with negative crystal shape. Compositions of inclusions 314-Q4-1 and 314-Q5-1 are listed in Table 2. Transitional (elongate but partly faceted) inclusion was heated at 900 °C and atmospheric pressure, but revitrification was incomplete, leaving several large vapor bubbles. All inclusions are shown at the same scale. Vapor bubbles are represented as black circles; other markings in these inclusions reflect incompletely revitrified daughter phases on walls.

→

Tiny euhedral quartz crystals

The third quartz population, found in the tephra and in surficial pumice and obsidian from the aphyric portion of the lava flow, is of small, fresh, euhedral bipyramidal crystals (Fig. 2c), which generally range from 250 to 580 μm in length (Fig. 3). They show no evidence of dissolution of the outer surfaces: faces, interfacial edges, and apices are all regular, pristine, and sharp, and the crystals reflect light like faceted diamonds, which they resemble. As seen in the intermediate euhedral quartz, some of these tiny euhedral crystals show starvation hollows at the centers of pyramidal faces, but in the fresh, tiny quartz crystals these hollows remain shallow and appear unmodified by any dissolution (see Fig. III-C, D of Clocchiatti and Mervoyer 1976).

Melt inclusions in the tiny euhedral quartz have diverse forms. The largest inclusions (from 30 to roughly 120 μm in length) are highly irregular, ranging from ovoids through elongate "peanut shell" and "boomerang" shapes (Figs. 4b and 4c). The smallest melt inclusions have negative crystal shapes (Figs. 4b and 5); a similar relation is seen in synthetically produced, secondary aqueous fluid inclusions in quartz, where in a given sample the smallest inclusions tend to be the most regularly shaped (Sterner and Bodnar 1984). Figure 6c shows that with decreasing inclusion size there is a distinct change in morphology from irregular to negative crystal shape around 30 μm in length. There are a few exceptions to this: six small inclusions have spherical or irregular shapes, some of which also show slight faceting, and three inclusions seem transitional, partly faceted but with elongate shapes.

Discussion

The three populations of quartz phenocrysts found in products of the rhyolitic Badlands lava-flow eruption reveal details of how crystal shapes and melt-inclusion morphologies can change with time. These relations also provide information on the state of the magma chamber, and the processes within it, before it was tapped by the eruption.

The large corroded quartz crystals remained at magmatic temperature sufficiently long that all their melt inclusions matured to negative crystal shapes. The size, abundance, and resorption features of the quartz and other phenocrysts indicate that the phenocryst-rich magma had an extended history, involving one or more changes in temperature, pressure, or composition conditions long before eruption. If resorption of the large corroded quartz crystals was caused by a change in external melt com-

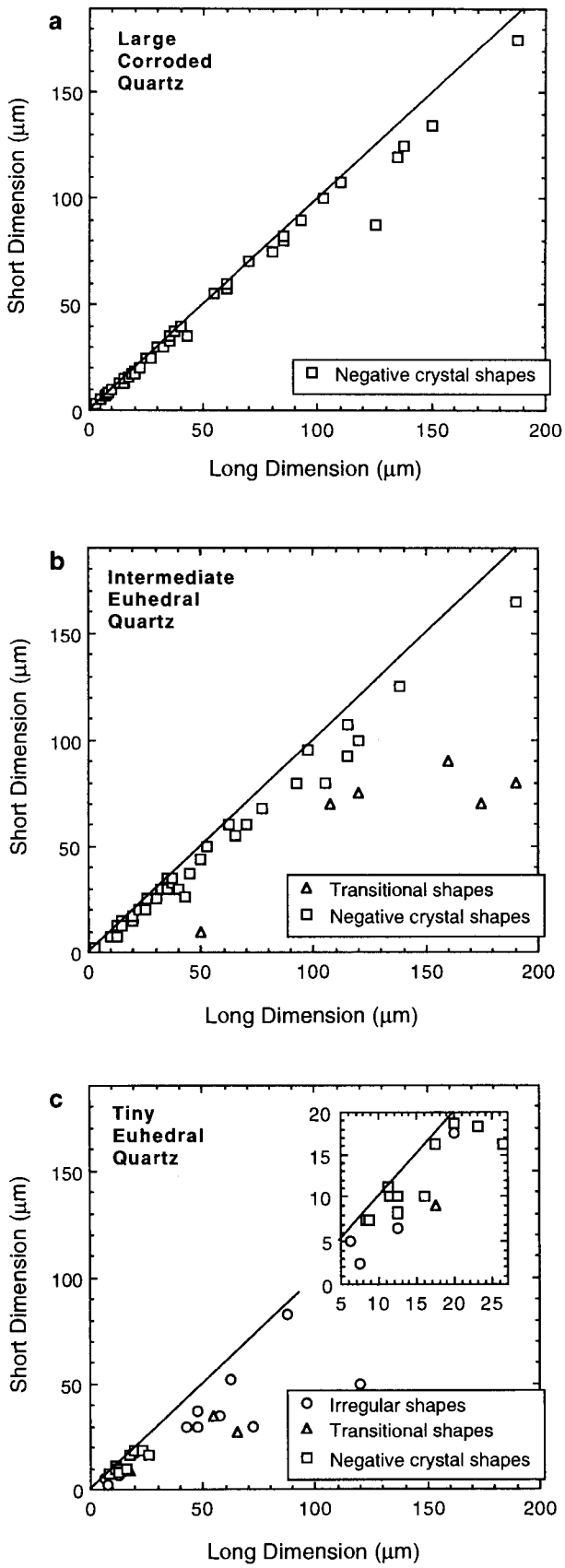

Figure 6. Relations between melt-inclusion shape and inclusion size. Plots of melt-inclusion size (long vs. short dimension) showing the variation of inclusion shape with size. Diagonal lines indicate long to short dimension ratios of 1:1. (**a**) Melt inclusions in the large corroded quartz population. All inclusions have negative crystal shapes. (**b**) Melt inclusions in the intermediate euhedral quartz population. Nearly all inclusions have negative crystal shapes, and none are irregular. The transitional inclusions are more strongly faceted than the transitional shapes in the tiny euhedral quartz crystals but are highly nonequidimensional. (**c**) Melt inclusions in the tiny euhedral quartz population, apparently growing just before the eruption. The largest inclusions are irregular in shape or transitional (partly faceted but without the equidimensional negative crystal shape). True bipyramidal, negative crystal shape is restricted to inclusions <30 μm in length; a few smaller inclusions of the other shapes are also <30 μm in size.

←

position, the melt inclusions should not have been affected. If, on the other hand, resorption was caused by a rise in temperature or drop in pressure (Nelson and Montana 1992), the inclusions may have become irregular at that time as well. Even if exterior conditions or lack of sufficient time did not allow the crystals to return to an equilibrium morphology, their inclusions, smaller and isolated from exterior conditions, were nonetheless able to mature back to negative crystal shapes.

The high degree of fracturing of the phenocrysts also raises the possibility that the magma had once nearly or completely solidified (during which time the phenocrysts were deformed) and was later remelted (e.g., Bacon et al. 1989). Differences in trace element contents (Manley 1994) between the melts (now matrix glasses) of the two lavas indicate that the phenocryst-rich magma was not produced by syneruptive mixing of disrupted cumulate crystals from the magma-chamber wall into the aphyric magma, as has been noted by Nakada et al. (1994) for a suite of rhyodacite lavas elsewhere.

In the tiniest euhedral quartz crystals, which must be the youngest of the quartz populations, the larger melt inclusions apparently did not have enough time to mature before eruption quenching froze-in their irregular, presumably initial shapes. Only the smallest inclusions in these tiny crystals had sufficient time at high temperature to mature to smooth, bipyramidal, negative crystal shapes.

Though the intermediate-sized euhedral quartz crystals are clearly related by size and morphology to the tiny euhedral crystals, even their very large melt inclusions nonetheless had sufficient time at magmatic conditions to mature.

The field and petrologic observations indicate that the Badlands magma chamber was stratified, with two layers (at least) of aphyric magma underlain by the phenocryst-rich magma (Fig. 1). The fresh morphology of the tiny euhedral quartz crystals show they were growing, in the aphyric magma closest to the chamber roof, shortly be-

fore being erupted; their presence in the tephra that erupted earliest, which vented rapidly, shows that they did not nucleate in response to initiation of eruption. The intermediate euhedral quartz crystals ceased growth before the eruption and were probably in equilibrium in the melt; these crystals resided in nearly aphyric magma presumably below that containing the tiny euhedral crystals.

Though it is likely that all the quartz crystals attained their present forms at depth in the chamber some time before the initiation of the Badlands eruption, there are no constraints on the absolute length of time any of the crystal populations resided in the magma. The size and freshness of the tiny euhedral quartz crystals and the irregular shape of their melt inclusions, however, suggest that their residence time may have been as brief as several weeks to several months. If this is the case, the eruption interrupted active differentiation in the Badlands magma chamber.

The distinct size ranges of the two populations of euhedral quartz and the apparent restriction of the populations to different layers in the preeruptive magma chamber also hint that the process that produced the evolved aphyric magma was episodic rather than continuous.

Melt-inclusion compositions

Large corroded quartz crystals

Compositions of two groups of melt inclusions from the large corroded quartz phenocrysts were analyzed: natural glassy inclusions and coarsely crystallized inclusions revitrified in the laboratory. Whole and fragmented quartz phenocrysts from the Badlands tephra contain melt inclusions that were quenched to glass during the explosive eruption; no revitrification was needed to analyze these inclusions. Inclusion glasses have silica contents ranging from 76.2 to 77.1 wt% (normalized anhydrous, Table 2), which is very similar to the matrix melt of the phenocryst-rich lava (Table 1), presumed to be little different from the melt from which the inclusions were originally trapped. The negative crystal shapes imply that silica was redistributed within and around the inclusions, but there is no compositional or textural evidence for growth of quartz or other daughter minerals at the expense of inclusion composition or volume.

Quartz phenocrysts from a sample of the basal vitrophyre of the Badlands lava flow contain inclusions that crystallized coarsely during slow cooling of the lava. These inclusions were revitrified at temperatures from 900 to 920 °C, at either atmospheric pressure or pressures of 230 or 530 MPa (2.3 or 5.3 kbar), in an internally heated, argon gas pressure vessel (see Holloway 1971), for 8–20 h. They show variable glass compositions that range from 67.5 to 76.5 wt% SiO_2 (normalized anhydrous), with other elements affected accordingly (Table 2).

Intermediate euhedral quartz crystals

Inclusions in the intermediate euhedral crystals, found only in the tephra, were quenched during their explosive eruption and thus remained glassy, though a discrete iron titanium oxide daughter-mineral grain grew in one inclusion (225-Q6-1), and several others developed incipient crystallite growth. A few of these inclusions were therefore revitrified at 900 °C and atmospheric pressure for 23 h. No significant compositional differences are apparent between inclusions that were revitrified and those that were not. The inclusion glasses have normalized silica contents of 75.9–78.0 wt% (Table 2) and uniform concentrations of other elements; they are essentially identical to the melt from which the host crystals presumably grew, now represented by the aphyric lava (90–188, Table 1).

Growth of the iron titanium oxide daughter mineral in inclusion 225-Q6-1 predictably lowered the Fe content of the melt (Table 2). Loss of silica by crystallization along the wall of the host apparently occurred along with growth of the oxide grain because melt silica is low and other elements show increases.

One of the inclusions of transitional shape was also analyzed (Manley unpublished data); its composition differs in no significant way from the other inclusion (of negative crystal shape) in the same host, nor from inclusions in the other hosts (Table 2).

Tiny euhedral quartz crystals

With one exception, the irregularly shaped inclusions in the tiny euhedral quartz population show no evidence of crystallization of discrete daughter-mineral grains. All eight analyzed inclusions are from samples of lava-flow carapace pumice that cooled slowly enough for the inclusion glass to become finely crystalline. Thus, the inclusions were revitrified at 900 °C for 22 h at atmospheric pressure. Inspection of the inclusions before and after revitrification showed that their shapes were not changed by the heating. Analyzed inclusions (33–120 μm in length) show normalized silica contents (Table 2) from roughly 77 to 78 wt%; this is identical to the melt from which the host crystals grew (90–188, Table 1).

One irregularly shaped melt inclusion, 62 × 52 μm in size (inclusion 314-Q5-1), shows the effects of crystallization of quartz along the wall of the inclusion. After revitrification, the glass of this inclusion appeared homogeneous and clear, though crystallized material was visible along the inclusion wall, and the vapor bubble remained larger than average. Silica contents are low and variable: two electron microprobe analyses of different portions of the inclusion indicate 68.7 and 70.3 wt% SiO_2, with other oxides correspondingly higher (Table 2).

None of the inclusions with negative crystal shape in the tiny euhedral crystals were sufficiently large to analyze on the ion microprobe at the time of the study; thus, they were also not analyzed by electron microprobe.

Discussion

The textural and compositional character of the Badlands melt inclusions clearly indicates that the trapped melt of the inclusions is not measurably modified as host

TABLE 2. Compositions of silicate melt inclusions from the Badlands rhyolite

	Inclusions of irregular shape				Inclusions of negative crystal shape		
	Tiny euhedral quartz				Intermediate euhedral quartz		
	Finely crystalline Revitrified at 900 °C				Glassy Not revitrified		
	Clear glass		Growth on wall		Brown/clear glass with oxide		
Group size	$n = 7$		$n = 1$		$n = 2$		$n = 1$
Sample	314	314	314		225	227	225
Inclusion	Q1-1	Q4-1	Q5-1		Q3-1	Q5-1	Q6-1
Analysis	15	19	20	21	17	22	15
SiO_2	76.9	78.0	68.7	70.3	76.2	76.3	73.8
TiO_2	0.12	0.12	0.08	0.13	0.15	0.15	0.08
Al_2O_3	11.0	10.8	16.4	15.2	12.4	12.3	14.5
Fe_2O_3**	1.35	1.15	0.98	1.28	1.80	1.58	0.45
MnO	<0.05	<0.05	<0.05	<0.05	<0.05	<0.05	<0.05
MgO	<0.01	0.02	<0.01	<0.01	0.02	0.05	<0.01
CaO	0.49	0.50	0.80	0.67	0.57	0.56	0.27
Na_2O	5.01	4.50	6.43	5.90	3.28	3.37	3.96
K_2O	4.65	4.52	5.87	5.82	5.27	5.30	6.06
P_2O_5	<0.03	<0.03	<0.03	0.05	<0.03	<0.03	0.07
Cl	0.12	0.10	0.13	0.09	n.a.	n.a.	n.a.
F	0.25	0.35	0.60	0.50	0.28	0.38	0.82
Total	98.90	97.51	100.75	100.60	99.52	97.53	102.13
H_2O	2.38	1.56	n.a.	n.a.	2.09	2.66	1.08

Note: Analyses recalculated to 100% anhydrous; totals are those before normalization. H_2O analyses by secondary ion mass spectrometry (SIMS or ion microprobe; see Hervig et al. 1989); all other oxides by electron microprobe. All data in weight percent; n.a. = not analyzed.

* Includes some compositionally identical glassy melt inclusions in large sanidine hosts.

** Total Fe as Fe_2O_3.

quartz dissolves and reprecipitates during the change from irregular to negative crystal shapes. In the Badlands inclusions, growth of other daughter minerals after trapping depletes the melt of those elements incorporated by the growing crystals and may also trigger loss of silica to the inclusion wall. Slow cooling from magmatic temperatures of the inclusions in the large corroded quartz crystals from the interior of the lava flow caused coarse-grained crystallization of the melt and significant loss of silica to the host quartz (see also Webster and Duffield 1991). This last process was responsible for the most serious changes to inclusion composition, as the silica that was lost to the quartz host is only very slowly remelted during revitrification of the inclusions in the laboratory. Even in revitrified inclusions that appear clear and glassy, significant compositional gradients can remain even after heating at 920 °C for up to 20 h (cf. Skirius et al. 1990). Because of such inhomogeneity, determining the original concentrations of other elements by correcting for silica loss (Webster and Duffield 1991) will not be completely successful for these inclusions.

CONCLUSIONS

Primary inclusions of rhyolitic melt in three distinct, apparently successive populations of quartz phenocrysts from the Badlands lava flow in southwestern Idaho illustrate a change from irregular to mature, negative crystal shapes. This process minimizes the surface energy of the inclusion by the solution and reprecipitation of quartz from the inclusion wall. In the quartz population growing just before the eruption, only the smallest melt inclusions, which would mature most quickly, show negative crystal shapes. In these, the larger melt inclusions are irregular, with shapes ranging from ovoid to "boomerang," probably the shapes these inclusions had at the time of trapping. Inclusions in a population of larger quartz crystals, which had nucleated earlier but ceased growth, all show either negative crystal shapes or faceted but elongate shapes presumably transitional to negative crystal shapes. All inclusions in a third population of even larger, very corroded quartz crystals, which spent significantly more time at magmatic temperatures, have mature negative crystal shapes regardless of inclusion size.

These considerations should apply to other silicic magmatic systems as well. Inclusions with irregular or nonmatured shapes may reveal phenocrysts that were forming just before their eruption or in which, in some cases, nucleation was triggered by, or along with, the eruption itself. In ideal cases, melt-inclusion and host-crystal morphology relations might help reveal the course or the causes of the eruption where other evidence has not been preserved or is inconclusive. For volcanic systems of more mafic compositions, growth of phenocrysts and formation of melt inclusions often continue during the eruption and afterward, during emplacement of lava flows. For-

TABLE 2.—*Continued*

Inclusions of negative crystal shape							
Intermediate euhedral quartz		Large corroded quartz					
Glassy Revitrified at 900 °C		Glassy Not revitrified		Coarsely crystalline Revitrified at 900 to 920 °C			
Clear glass		Clear glass		Clear glass with remnant daughter crystals			
$n = 6$		$n = 12$*		$n = 12$		$n = 1$	
225 Q11-1	225 Q12-2	225 Q2-1	225 Q1-3	164 Q33-1	164 Q1-1	164 Q40-1	
9	12	8	7	8	23	12	10
75.9	78.0	76.2	77.1	67.5	76.5	70.2	75.3
0.10	0.08	0.13	0.13	0.20	0.10	0.15	0.15
12.2	11.1	12.7	12.2	16.1	10.8	15.3	12.0
1.45	1.33	1.54	1.41	2.64	2.74	1.63	1.98
<0.05	<0.05	<0.05	<0.05	0.05	<0.05	<0.05	<0.05
<0.01	<0.01	0.02	0.02	0.05	0.05	<0.01	0.03
0.60	0.51	0.53	0.47	1.00	0.57	0.81	0.53
4.22	3.92	3.60	3.28	5.89	3.85	5.24	3.97
5.02	4.70	5.21	5.29	6.24	5.06	6.20	5.77
<0.03	<0.03	<0.03	<0.03	<0.03	<0.03	<0.03	<0.03
0.11	0.12	0.09	0.07	n.a.	n.a.	n.a.	n.a.
0.31	0.28	n.a.	n.a.	0.34	0.33	0.41	0.29
99.06	97.58	96.71	96.85	101.25	99.67	99.33	99.61
3.60	2.20	3.06	2.66	0.73	2.32	4.55	2.47

tuitous conditions and careful sampling may permit pre- and posteruptively trapped inclusions to be studied to reveal compositional changes accompanying eruption. For such mafic magmas, in which inclusions would be trapped in phases other than quartz, relationships similar to those documented here for rhyolitic quartz-hosted inclusions would need to be confirmed.

Electron microprobe analyses of the various populations of inclusions also confirm that maturation of inclusions has no effect on the composition of the trapped melt, at least in these rhyolitic inclusions in quartz phenocrysts. After eruption, however, those inclusions that cooled most slowly lost silica to quartz growth on the inclusion walls and to coarse crystallization in the body of the inclusion. Although such crystalline inclusions were revitrified to clear glass in the laboratory, silica contents remained low and variable, and other elements high, indicating that the inclusions did not regain all lost silica and did not become homogeneous. Other inclusions, which cooled more quickly but nonetheless became finely crystalline and needed to be revitrified to clear glass, showed no such loss of silica to the quartz host.

In the study of silicic melt inclusions from older eruptions, the age of the eruption is much less important than the cooling rates of the inclusions immediately after. If the inclusion cooled quickly once it reached the surface, and if it was not significantly reheated later, very old (perhaps even Precambrian) inclusions may be candidates for microbeam analysis.

ACKNOWLEDGMENTS

Discussions about melt inclusions with Richard Hervig, Jacob Lowenstern, and Kurt Roggensack were very helpful. I am grateful to John Holloway for allowing me to use laboratory equipment and sample preparation facilities, and to Ken Domanik for invaluable assistance with the internally heated, gas pressure vessel during the high-pressure revitrification of certain of the melt inclusions. Richard Hervig provided advice, instruction, and assistance with the ion microprobe, and Jim Clark assisted with electron microprobe analyses. Reviews by Eric Christiansen, Richard Hervig, and Virginia Sisson greatly improved the manuscript. Various portions of this research were supported by Geological Society of America research grant 4266–89, a Stanford School of Earth Sciences McGee Fund grant, and NSF grants EAR-9018216 to R. Hervig and EAR-9105329 to Jonathan Fink.

REFERENCES CITED

Andersen, D.J., Lindsley, D.H., and Davidson, P.M. (1993) QUILF: A PASCAL program to assess equilibria among Fe-Mg-Mn-Ti oxides, pyroxenes, olivine, and quartz. Computers and Geosciences, 19, 1333–1350.

Bacon, C.R., Adami, L.H., and Lanphere, M.A. (1989) Direct evidence for the origin of low-^{18}O silicic magmas: Quenched samples of a magma chamber's partially-fused granitoid walls, Crater Lake, Oregon. Earth and Planetary Science Letters, 96, 199–208.

Beddoe-Stephens, B., Aspden, J.A., and Shepherd, T.J. (1983) Glass inclusions and melt compositions of the Toba Tuffs, northern Sumatra. Contributions to Mineralogy and Petrology, 83, 278–287.

Blake, S., and Ivey, G.N. (1986) Magma mixing and the dynamics of withdrawal from stratified reservoirs. Journal of Volcanology and Geothermal Research, 22, 1–31.

Bonnichsen, B. (1982a) The Bruneau-Jarbidge Eruptive Center, southwestern Idaho. In Idaho Bureau of Mines and Geology Bulletin, 26, 237–254.

——— (1982b) Rhyolite lava flows in the Bruneau-Jarbidge Eruptive Cen-

ter, southwestern Idaho. In Idaho Bureau of Mines and Geology Bulletin, 26, 283–320.

Bonnichsen, B., and Kauffman, D.F. (1987) Physical features of rhyolite lava flows in the Snake River Plain volcanic province, southwestern Idaho. In Geological Society of America Special Paper, 212, 119–145.

Chaigneau, M., Massare, D., and Clocchiatti, R. (1980) Contribution à l'étude des inclusions vitreuses et des éléments volatils contenus dans les phénocristaux de quartz de roches volcaniques acides. Bulletin Volcanologique, 43, 233–240.

Clocchiatti, R. (1975) Les inclusions vitreuses des cristaux de quartz: Etude optique, thermo-optique et chimique. Applications géologiques. Societe Géologique de France Memoires, LIV, Memoire 122, 96 p.

Clocchiatti, R., and Mervoyer, B. (1976) Contribution à l'étude des cristaux de quartz de la Guadeloupe. Bulletin du Bureau de Recherches Geologiques et Minieres, France, 2e série, sec. IV, 4, 311–324.

Clocchiatti, R., and Basset, A.M. (1978) Skeletal growth and melt inclusions in quartz crystals of rhyodacitic ignimbrites of the Valley of Ten Thousand Smokes, Katmai, Alaska. Eos, 59, 225.

Delaney, P.T., and Pollard, D.D. (1981) Deformation of host rocks and flow of magma during growth of minette dikes and breccia-bearing intrusions near Ship Rock, New Mexico. U.S. Geological Survey Professional Paper, 1202, 61 p.

Donaldson, C.H., and Henderson, C.M.B. (1988) A new interpretation of round embayments in quartz crystals. Mineralogical Magazine, 52, 27–33.

Ekren, E.B., McIntyre, D.H., and Bennett, E.H. (1984) High-temperature, large-volume, lavalike ash-flow tuffs without calderas in southwestern Idaho. U.S. Geological Survey Professional Paper, 1272, 76 p.

Fuhrman, M.L., and Lindsley, D.H. (1988) Ternary-feldspar modeling and thermometry. American Mineralogist, 73, 201–215.

Hervig, R.L., Dunbar, N., Westrich, H.R., and Kyle, P.R. (1989) Pre-eruptive water content of rhyolite magmas as determined by ion microprobe analyses of melt inclusions in phenocrysts. Journal of Volcanology and Geothermal Research, 36, 293–302.

Holloway, J.R. (1971) Internally heated pressure vessels. In G.C. Ulmer, Ed., Research techniques for high pressure and high temperature, p. 217–258. Springer-Verlag, New York.

Laporte, D., and Provost, A. (1994) The equilibrium crystal shape of silicates: Implications for the grain-scale distribution of partial melts. Eos, 75, 364.

Manley, C.R. (1994) On voluminous rhyolite lava flows, 314 p. Ph.D. thesis, Arizona State University, Tempe.

——— (1995) How voluminous rhyolite lavas mimic rheomorphic ignimbrites: Eruptive style, emplacement conditions, and formation of tuff-like textures. Geology, 23, 349–352.

McBirney, A.T. (1980) Mixing and unmixing of magmas. Journal of Volcanology and Geothermal Research, 7, 357–371.

Nakada, S., Bacon, C.R., and Gartner, A.E. (1994) Origin of phenocrysts and compositional diversity in pre-Mazama rhyodacite lavas, Crater Lake, Oregon. Journal of Petrology, 35, 127–162.

Nelson, S.T., and Montana, A. (1992) Sieve-textured plagioclase in volcanic rocks produced by rapid decompression. American Mineralogist, 77, 1242–1249.

Roedder, E. (1984) Fluid inclusions. In Mineralogical Society of America Reviews in Mineralogy, 12, 644 p.

Shelton, K.L., and Orville, P.M. (1980) Formation of synthetic fluid inclusions in natural quartz. American Mineralogist, 65, 1233–1236.

Sisson, V.B., Lovelace, R.W., Maze, W.B., and Bergman, S.C. (1993) Direct observation of primary fluid-inclusion formation. Geology, 21, 751–754.

Skirius, C.M., Peterson, J.W., and Anderson, A.T., Jr. (1990) Homogenizing rhyolitic glass inclusions from the Bishop Tuff. American Mineralogist, 75, 1381–1398.

Sterner, S.M., and Bodnar, R.J. (1984) Synthetic fluid inclusions in natural quartz: I. Compositional types synthesized and applications to experimental geochemistry. Geochimica et Cosmochimica Acta, 48, 2659–2668.

Turner, J.S., and Gufstafson, L.B. (1981) Fluid motions and compositional gradients produced by crystallization or melting at vertical boundaries. Journal of Volcanology and Geothermal Research, 11, 93–125.

Webster, J.D., and Duffield, W.A. (1991) Volatiles and lithophile elements in Taylor Creek Rhyolite: Constraints from glass inclusion analysis. American Mineralogist, 76, 1628–1645.

Wilkins, R.W.T. (1979) Formation, modification and destruction of fluid inclusions: Notes for fluid inclusion workshop. Department of Geology, La Trobe University, La Trobe, Bundoora, Victoria, Australia, February 1979 (mimeographed, 8 p.) (as referenced by Roedder 1984).

Wortis, M. (1988) Equilibrium crystal shapes and interfacial phase transitions. In R. Vanselow and R.F. Howe, Eds., Chemistry and physics of solid surfaces VII, p. 367–405. Springer-Verlag, New York.

Manuscript received October 3, 1994
Manuscript accepted September 1, 1995